Journal of Electrical Engineering & Technology (2020) 15:2099–2110
https://doi.org/10.1007/s42835-020-00508-4

ORIGINAL ARTICLE

Multi-terminal Medium Voltage DC Distribution Network Large-signal Stability Analysis

Patrobers Simiyu[1] · Ai Xin[1] · Niasse Mouhammed[1] · Wang Kunyu[1] · Joseph Gurti[1]

Received: 2 May 2020 / Revised: 21 July 2020 / Accepted: 3 August 2020 / Published online: 10 August 2020

Abstract
The Brayton-Moser's mixed potential theory is a popular approach for large-signal stability analysis of DC-based systems with constant power load (CPL). The criterion from the conventional mixed potential theory contains multiple time-varying parameters which are complicated for convenient stability analysis hence the need for simplification. On the other hand, stability analysis of droop-controlled multiple source converter-based DC systems are scarce. Thus, the large-signal stability criterion of a scaled-down droop-controlled multi-terminal MVDC distribution network with CPL using Brayton-Moser's mixed potential theory was simplified and derived to show that CPL power rating, PI control parameters, droop and damping coefficients have profound effects on the system's large-signal stability. By way of MATLAB/Simulink simulations, the large-signal stability of the MVDC distribution system was observed to reduce with increase in CPL power rating and source converter droop coefficients as well as increase with increase in proportionate coefficient values and use of optimized unlike non-optimized damping coefficients. Therefore, the droop-controlled MVDC distribution network with optimized PI control parameters, droop and damping coefficients have enhanced dynamic response and large-signal stability margin proving the accuracy and validity of the simplified large-signal stability criterion.

Keywords CPL · DC voltage droop · Large-signal stability · MVDC distribution network · Mixed potential theory

1 Introduction

Advances in VSC and cable technologies are paving way for new electricity market requirements in favor of multi-terminal VSC–MVDC distribution network integration in commercial and industrial applications [1, 2]. The MVDC distribution network typically rated 1.5–30 kV, offers power systems' solutions like de-risking VSC-HVDC transmission systems, AC distribution network reinforcements, renewable energy (RE) integration, railway system applications, urban electrification etc. [2–5]. Its feasibility has been proven extensively in many researches in the US [6], Germany [7], China [8] amongst others from which several aspects have emerged as hot research topics namely; dynamic DC voltage control, MVDC network stability analysis, MVDC system protection investigations and distributed energy resource (DERs) integration [2, 7, 8].

In a multi-terminal MVDC distribution system, energy sources and loads are connected to the DC distribution bus via power converters [1, 6]. Typically, a converter works under closed-loop control with non-linear dynamic behavior due to its electronic switching devices. Usually, each converter is designed to be stable as a stand-alone unit. However when converters are interconnected on the same DC bus, they exhibit nonlinear behavior that adds an extra element of complexity to the overall system dynamics. When observing the system from the DC bus, the load converters operating under closed-loop output voltage control display constant power load (CPL) characteristics that contrasts the voltage-current characteristic of the classical resistive load. This CPL effect is a non-linear behavior that causes the equivalent incremental negative input resistance that leads to a destabilizing subsystem's interaction problem [9–11].

Many stability studies involving CPL in DC microgrids have been investigated using small-signal analysis approaches [12–14]. The most popular small-signal stability analysis methods are the eigenvalue analysis and

✉ Patrobers Simiyu
simiyupr@yahoo.com

[1] State Key Laboratory of Alternate Electric Power Systems With Renewable Energy Sources, North China Electric Power University, Beijing 102206, China

the impedance-based criteria in which the DC system is linearized around an equilibrium point. However, the feasibility of the small-signal analysis is only limited to system assessments under small disturbances [14, 15] such as load variations or slow parameters changes etc. that are quite small that linearization of the system model does not affect the accuracy of the stability analysis. Contrastingly, large disturbances, such as loss of power generation unit, load switching, large variations in load, load rejection, CPL effect, short-circuit fault and open lines happen from time to time during actual system operation. The large disturbances subject the system into transients where no certain equilibrium point exists making small-signal stability analysis ineffective [16]. Naturally, a large-signal stability system is small-signal stable but the converse is not certainly true, as large-signal analysis takes into account the nonlinear characteristics of the system whereas the small-signal analysis does not [17]. In this way, studying large-signal stability of an MVDC distribution network is crucial for overall system's stability.

Several research works have been done on large-signal stability analysis in DC systems [18], such as the Lyapunov direct method [19], the Takagi–Sugeno fuzzy modelling method (TS) [16, 19], the block-diagonalized quadratic Lyapunov function (BDQLF) [20], the reverse trajectory tracking method [18, 21], the Hamiltonian surface shaping method [22] and the mixed potential theory [23, 24] amongst others. The Lyapunov direct method is the most widely applied circuit parameter based large-signal analysis method. It is capable of estimating the region of asymptotic stability (RAS) of an operating point with conservative results. Besides, the construction of a Lyapunov function; a locally positive definite scalar function about the equilibrium point is yet to receive consensus leaving room for non-uniformity in its formulation. The TS and BDQLF are the derivatives of the Lyapunov direct method, hence share similar problems of giving conservative RAS estimates. In addition, the TS computational burden increases exponentially with the number of nonlinearities, making it ineffective for higher-order systems. The reverse trajectory tracking approach is designed to yield the most accurate RAS estimations. However, it is fundamentally a graphical method which cannot present the RAS estimate in an analytical form hence impractical for higher-order systems. The Hamiltonian surface shaping method derives its stability approximations without accounting for the influence of controller parameters on system's stability. It can be observed that none of the five methods provide a large-signal stability criterion in an analytical form covering both circuit and controller parameters. In contrast, the mixed potential theory, provides a large-signal stability criterion involving circuit and controller parameters in an analytical form hence more appropriate stability tool for DC grids [16, 18–24].

Different large-signal stability studies on DC power systems have been undertaken using Brayton-Moser mixed potential theory. Authors in [25] developed a design-oriented mixed potential theory criterion for a DC distributed system with CPL to guarantee large-signal stability. Large-signal stability analysis of 'more electric aircraft' systems with CPL was undertaken using mixed potential theory alongside Lyapunov stability theorems and estimation of the system's RAS obtained using LaSalle invariance principle in [26–28]. In [29], the mixed potential theory is applied to investigate the influence of multistage LC filter parameters on the large-signal stability of a DC system with CPL. In [17], the mixed potential function of a cascaded system is determined and the influence of control parameters on the large-signal stability examined. The mixed potential function of a bidirectional DC–DC converter in the bucking mode with CPL is ascertained and the impact of controller limitations on large-signal stability investigated in [30]. The large-signal stability criterion based on the mixed potential theory is derived in [31], and the investigations found coincident with Hopf bifurcation stability analysis. In the aforementioned researches, the DC bus voltage is controlled by one converter while studies involving stability of multiple converters under droop control remain scarce hence the need for more investigations.

Increasing penetration of power converter-based systems (PCBS) deteriorates the equivalent inertia and damping risking the stability of power system. Thus, virtual inertia/synthetic inertia implemented in the primary control strategy of the PCBS that enables it imitate the inertia response of the conventional synchronous generator was proposed to improve the dynamic response and stability of the system [32]. In AC and DC networks, the virtual inertia facilitates frequency regulation as well as control variations in DC voltage respectively [33–35]. In the multi-terminal MVDC distribution network as a typical PCBS, integration of virtual inertia in its droop-based scheme in [36] improve accuracy of power sharing in the VSCs as well as regulate DC voltage deviations with enhanced damping and dynamic response.

Therefore, this paper analyzes the large-signal stability of a droop-controlled multi-terminal MVDC distribution network with CPL. The paper is organized as follows; Sect. 2 outlines the MVDC distribution grid structure. The Brayton–Moser's mixed potential theory on large-signal stability is outlined in Sect. 3. Section 4 presents droop control with virtual inertia. The particle swarm optimization (PSO) algorithm for the MVDC network control parameters is outlined in Sect. 5. In Sect. 6, the simulation results are given. Lastly, Sect. 7 draws the conclusion.

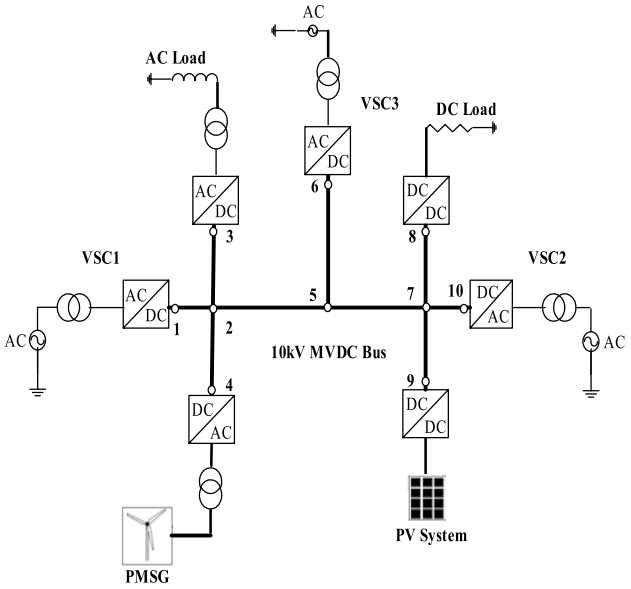

Fig. 1 0 MVDC Distribution Network

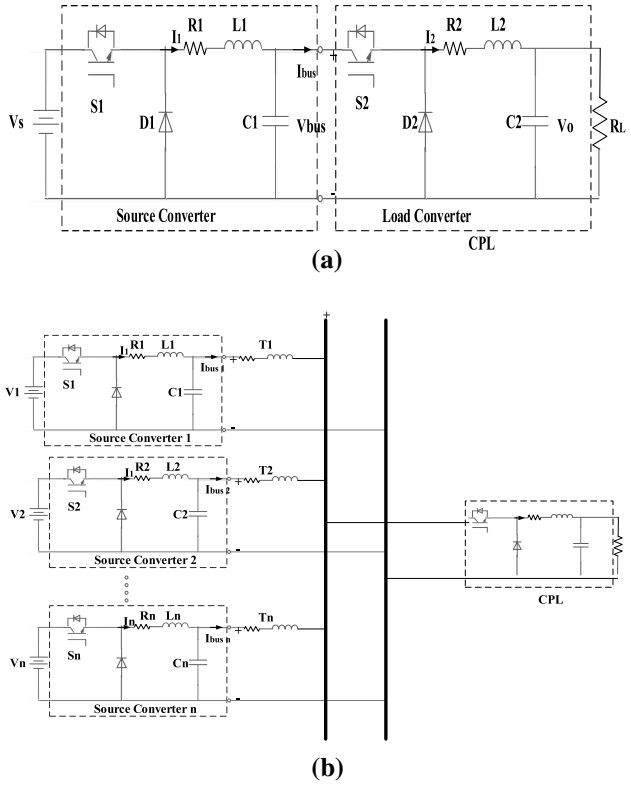

Fig. 2 Cascaded Converters (**a**) Single Source-Load (b) Multiple Source-Single Load

2 MVDC Distribution Network Structure

In Fig. 1, the droop-controlled multi-terminal MVDC distribution network under investigation is shown. The MVDC bus facilitates the interaction of the AC grids, wind power unit and solar PV, as well as AC and DC loads [36]. The wind generator operates on constant power while the PV system works at maximum power point tracking (MPPT) mode hence both REs are seen as a lumped constant power source (CPS). The AC and DC loads are typical CPLs. The CPS is seen as a negative CPL hence together with typical CPLs are represented as a lumped CPL [37]. As a result, the system can be reduced to a cascaded connection of power converters in which the power source supplies the DC bus through the source converter whereas the load consumes from the bus via a load converter. The use of buck converters is popular in many studies involving such forms of cascaded systems including DC microgrids [17, 37, 38]. Figure 2 shows the simplified MVDC distribution network topology and the equivalent circuit for large-signal stability studies.

Assuming the basic model in Fig. 2a; the state-space equations for the system can be given as;

$$\begin{aligned} L_1 \frac{di_1}{dt} &= d_1 v_1 - r_1 i_1 - v_{bus} \\ \mathrm{C}_1 \frac{dv_{bus}}{dt} &= i_1 - i_{bus} \end{aligned} \tag{1}$$

$$\begin{aligned} L_2 \frac{di_2}{dt} &= d_2 v_{bus} - r_2 i_2 - v_0 \\ \mathrm{C}_2 \frac{dv_0}{dt} &= i_2 - \frac{v_0}{r_L} \end{aligned} \tag{2}$$

where d_1 and d_2 are the duty cycles of the buck converters 1 and 2 respectively.

3 Brayton-Moser's Mixed Potential Theory Criterion on Large-Signal Stability

The mixed potential theory was proposed under the general assumptions of the Kirchhoff's laws for constructing the Lyapunov function of a system for large-signal stability analysis. The approach is used in estimating a large region containing the equilibrium point and the RAS. This approach shows the dynamics of a nonlinear circuit in which every branch current and voltage can be obtained from a set of inductor currents and capacitor voltages. The network can be described by the differential equations [23] as follows:

$$L\frac{di_\rho}{dt} = \frac{\partial P(i,v)}{\partial i_\rho}$$
$$C\frac{dv_\sigma}{dt} = -\frac{\partial P(i,v)}{\partial v_\sigma} \quad (3)$$

where P(i,v) is a scalar mixed potential function of the network used to build the Lyapunov energy function for the nonlinear system, i is the current in the inductors, v is the voltage of the capacitors, L and C are the nonlinear current and voltage dependent matrices respectively containing inductance and capacitance. It should be noted that the mixed potential function relates the distribution circuit structure of the inductor, capacitor and non-storage element.

The mixed potential function can be expressed to account for the current potential function of the non-energy storage element as well as the energy of the capacitor branch as;

$$P(i,v) = \int \sum_{\mu>r+s} v_\mu di_\mu + \sum_{\sigma=r+1}^{r+s} i_\sigma v_\sigma \quad (4)$$

where r and s are the number of inductor and capacitor branches respectively. The mixed potential function can be constructed according to (4) using the procedure below:

i. Calculate the current potential function of all non-energy storage elements in the circuit.
ii. Calculate the energy contained in the capacitive element i.e. the product of current and voltage for all capacitor branches.
iii. Add (i) and (ii) to get the mixed potential function.

Thus the general mixed potential function is given as.

$$P(i,v) = -A(i) + B(v) + (i, \gamma v - \alpha) \quad (5)$$

where A(i) and B(v) are current and voltage potential function respectively, γ.is the circuit topology based constant matrix with elements ± 1 depending on the nature of the network topology, whereas α is a constant vector.

The mixed potential function has three related stability theorems for large-signal stability of nonlinear circuits. The current and voltage potential functions are the first and second stability theorems respectively that are largely linear and inappropriate for this study. The third stability theorem gives a theoretical foundation for solving the stability boundary of the system subjected to large-signal disturbances. Thus the third theorem states that; if

$$\mu_1 + \mu_2 \geq \delta,\ \delta > 0 \quad (6)$$

for all i, v; then

$$P^*(i,v) = \frac{\mu_1 - \mu_2}{2}P(i,v) + \frac{1}{2}P_i^T L_s^{-1} P_i + \frac{1}{2}P_v^T C^{-1} P_v \to \infty \quad (7)$$

as $|i| + |v| \to \infty$. All the solutions of the system will tend to a stable equilibrium point as $t \to \infty$ guaranteeing large-signal stability, [24] where μ_1 and μ_2 are the smallest Eigen-values of the first order matrices $L^{-1/2} * A_{ii} * L^{-1/2}$ and $C^{-1/2} * B_{vv} * C^{-1/2}$ for all i and v respectively. Other terms are defined as;

$$P_i = \frac{\partial P(i,v)}{\partial i}; P_v = -\frac{\partial P(i,v)}{\partial v} \quad (8)$$

$$A_{ii}(i) = \frac{\partial^2 A(i)}{\partial i^2}; B_{vv}(v) = -\frac{\partial^2 B(v)}{\partial v^2} \quad (9)$$

Considering a droop controller in buck converter 1 in the cascaded system in Fig. 2(a), Fig. 3 can be drawn to illustrate the simplified system. The source converter incorporates a double closed-loop scheme whereas a load converter reduces to a CPL.

The control system of the source converter can be described using the following expressions; where R_d is the droop coefficient.

$$i_{1ref} = k_{vp}\left[V_{busref} - V_{bus} - R_d i_1\right] + k_{vi}\int_0^t \left[V_{busref} - V_{bus} - R_d i_1\right] dt$$
$$d_1 = k_{ip}\left[I_{ref} - i_1\right] + k_{ii}\int_0^t \left[I_{ref} - i_1\right] dt \quad (10)$$

The mixed potential function of the system can be written in the form similar to (4) as;

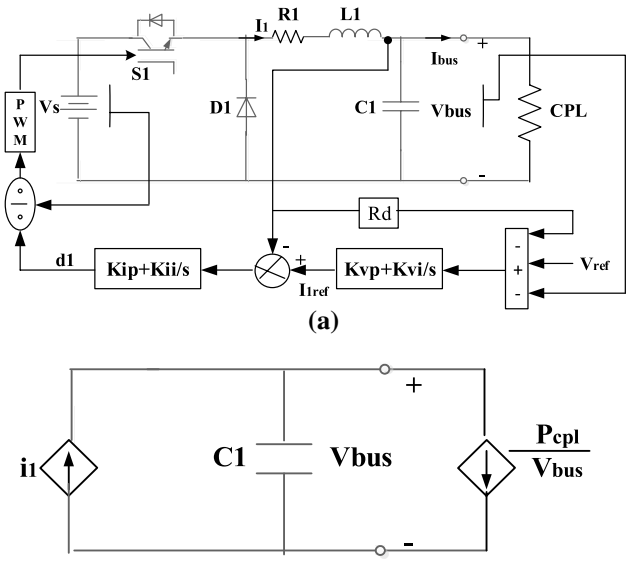

Fig. 3 Cascaded System; (**a**). Simplified (**b**). Equivalent Circuit

$$P(i,v)=\left(\int_0^{i_1} v_{bus}di_1-\int_0^{i_{bus}}\frac{P_{CPL}}{i_{bus}}di_{bus}\right)+\left(-v_{bus}\left[i_1-\frac{P_{CPL}}{v_{bus}}\right]\right)$$
$$P(i,v)=\left(v_{bus}i_1-\int_0^{v_{bus}} i_1dv_1-P_{CPL}+\int_0^{v_{bus}}\frac{P_{CPL}}{v_{bus}}dv_{bus}\right)+$$
$$\left(-v_{bus}i_1+P_{CPL}\right)$$
$$P(i,v)=\int_0^{v_{bus}}\frac{P_{CPL}}{v_{bus}}dv_{bus}-\int_0^{v_{bus}} i_1dv_{bus} \tag{11}$$

When (11) is introduced in (3), an accurate mixed potential theory function can be realized as;

$$-C_1\frac{dv_{bus}}{dt}=\frac{\partial P(i,v)}{\partial v_{bus}}=\frac{P_{CPL}}{v_{bus}}-i_1 \tag{12}$$

The mixed potential function can be transformed to an even expression in (5) as;

$$A(i)=0$$
$$B(v)=\int_0^{v_{bus}}\frac{P_{CPL}}{v_{bus}}dv_{bus}-\int_0^{v_{bus}} i_1dv_{bus} \tag{13}$$
$$i,\gamma v-\alpha=0$$

Rewriting in terms of (9) based on the third stability theorem results into;

$$A_{ii}(i)=\frac{\partial^2 A(i_1)}{\partial i_1^2}=0$$
$$B_{vv}(v)=\frac{\partial^2 B(v_{bus})}{\partial v_{bus}^2}=-\frac{P_{CPL}}{v_{bus}^2}-\frac{\partial i_1}{\partial v_{bus}} \tag{14}$$

From (1); i_1 is given by;

$$i_1=\frac{d_1v_1-v_{bus}}{r_1} \tag{15}$$

neglecting the time-varying item where d_1 is given in (10). Ignoring the integral terms in (10) d_1 can be substituted accordingly in (15) to give;

$$i_1=\frac{\left(v_1k_{ip}k_{vp}v_{busref}-v_{bus}\left[v_1k_{ip}k_{vp}-1\right]\right)}{r_1+v_1k_{ip}\left[k_{vp}R_d+1\right]} \tag{16}$$

The partial differentiation in (14) is given by;

$$B_{vv}(v)=\frac{\partial^2 B(v)}{\partial v_{bus}^2}=-\frac{P_{CPL}}{v_{bus}^2}+\frac{v_1k_{ip}k_{vp}}{r_1+v_1k_{ip}\left[k_{vp}R_d+1\right]} \tag{17}$$

Applying the mixed potential theorem for large-signal stability, the following relations are obtained;

$$u_1=\min\left[\lambda\left(L^{-0.5}A_{ii}L^{-0.5}\right)\right]=0$$
$$u_2=\min\left[\lambda\left(C^{-0.5}B_{vv}C^{-0.5}\right)\right]=-\frac{P_{CPL}}{v_{bus}^2}+\frac{v_1k_{ip}k_{vp}}{r_1+v_1k_{ip}\left[k_{vp}R_d+1\right]} \tag{18}$$

Based on (5), the criterion for large-signal stability is derived as;

$$\frac{P_{CPL}}{v_{bus}^2}<\frac{v_1k_{ip}k_{vp}}{r_1+v_1k_{ip}\left[k_{vp}R_d+1\right]} \tag{19}$$

where P_{cpl}, v_{bus}, v_1, K_{vp}/K_{ip}, r_1 and R_d represents the CPL rating, DC bus voltage, input voltage, the proportionate coefficient of the outer voltage and current control loops of the converter, parasitic resistance and the droop coefficient respectively.

4 Integrating Virtual Inertia Control

In this research work, virtual inertia is incorporated in the DC voltage droop control scheme of the MVDC distribution system. The converter integrated with virtual inertia have similar features as the synchronous generator swing equation in (20); where Sn is the synchronous generator rated capacity, H is the inertia time constant, J is the moment of inertia of the synchronous generator, ω is its mechanical angular velocity, T_m is the synchronous generator mechanical torque, T_e is its electromagnetic torque, T_d is its damping torque, D is its damping coefficient and ω_o is the synchronous angular velocity of the grid.

$$J\frac{d\omega}{dt}=T_m-T_e-T_d$$
$$J\frac{d\omega}{dt}=T_m-T_e-D(\omega-\omega_0)\text{ where }J=H\frac{S_n}{\omega_0^2} \tag{20}$$

The fundamental equation for the DC voltage droop controller is given by:

$$v=v_{ref}-R_d\left(i-i_{ref}\right) \tag{21}$$

where v is the measured voltage, v_{ref} is the reference voltage, R_d is the droop coefficient, i is the measured current and i_{ref} is the reference current. Reorganizing (21), the following expression is realized:

$$0=\left(i_{ref}-i\right)-\frac{1}{R_d}\left[v-v_{ref}\right] \tag{22}$$

Comparing the right-hand-side of (20) and (22); the 'torques' are analogous to 'currents' whereas 'velocities' are comparable to 'voltages.' In this way, the time derivative term of voltage i.e. across the capacitor side of the converter can be added to the left-hand side of (22), to give;

$$K_1 \frac{dv}{dt} = \left(i_{ref} - i\right) - \frac{1}{R_d}\left[v - v_{ref}\right] \tag{23}$$

where K_1 is a constant.

Rewriting (23), the following expression is realized:

$$v = v_{ref} - R_d\left(i - i_{ref}\right) - K_1 R_d \frac{dv}{dt} \tag{24}$$

where K_1R_d is a constant.

It can be realized that the time derivative of the voltage across the capacitor is proportional to the capacitor current. Therefore, replacing the last term on the right-hand-side in (24) gives;

$$v = v_{ref} - R_d\left(i - i_{ref}\right) - K_d i_c \tag{25}$$

where K_d is the damping coefficient in the virtual inertia-based controller and i_c is the capacitor current.

In this way, a negative feedback term $K_d i_c$ is used in the voltage control loop to provide a desirable amount of damping to improve the dynamic response of the droop-based controlled MVDC system with virtual inertia. When optimized K_d values derived from optimization algorithms are applied, the system's dynamic performance is considerably improved. In this study, particle swarm optimization (PSO) algorithm is used in MATLAB to find the optimal parameters for the PI controllers including the damping coefficient (K_d) of the system. Figure 4 shows the DC voltage droop with virtual inertia control.

5 Particle Swarm Optimization Algorithm

PSO algorithm offers a strong ability to solving problems characterized by nonlinearity/non-differentiability, multiple optima and high dimensionality. Its logic is derived from the swarming intelligence in flocks of birds, fish shoals or insects [39]. Consider a group of N individuals called particles that move together in steps in a defined region or solution space. At each step k, the objective function is evaluated for each particle then recorded along with its current position x_i. Before moving to the next step, the algorithm adjusts the velocity vector v_i of each particle towards a new position determined by the best position found by the swarm (g_b) and also by the particle itself (P_b). Subsequently, many studies have been carried out to improve the performance of the PSO regarding speed of convergence as well as make sure that the algorithm doesn't get stuck at a local minimum. The velocities and the positions of the particles can be updated using (26) and (27) [40, 41];

$$v_i^{k+1} = wv_i^k + c_1 r_1 (p_{bi} - x_i^k) + c_2 r_2 (g_{bi} - x_i^k) \tag{26}$$

$$x_i^{k+1} = x_i^k + v_i^{k+1} \tag{27}$$

where r_{12} are generated random numbers between [0,1]; c_{12} are the learning factors defined by the designer.

Designers have various choices when assessing the PI controller performance in the frequency-domain analysis. The criteria include the: integral squared error (ISE), integral time-weighted square error (ITSE), integral absolute error (IAE), and integral time-weighted absolute error (ITAE). Each of these integral performance criteria has its own advantages and limitations regarding error minimization rapidity, rise time, settling time, steady-state error, complexity and time-consumption of the analytical formula. The ITAE criterion presents a good compromise between a comparatively higher time performance (rise time) and a comparatively lower error-minimization performance (overshoot). Equation (28) shows the formula of ITAE criterion:

$$\text{ITAE} = \int_0^\infty t.|e(t)|\mathrm{d}t \tag{28}$$

In this paper, the ITAE is used for assessing the PI controller performance. Figure 5 shows the PSO optimization using ITAE. A set of good Kp and Ki control parameters will come with a minimal computed value of the chosen performance criterion in time domain including the overshoot, rise time, settling time, and steady-state error. Therefore, when controlling the dynamic frequency response of the system,

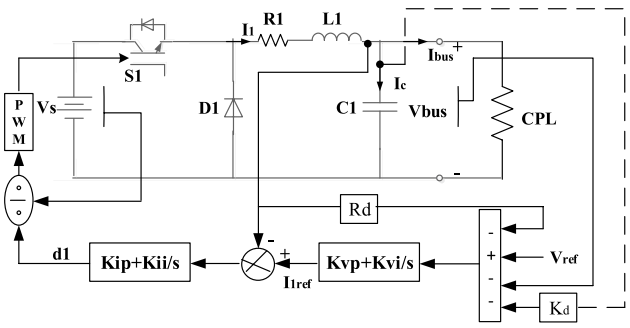

Fig. 4 DC voltage droop with virtual inertia control

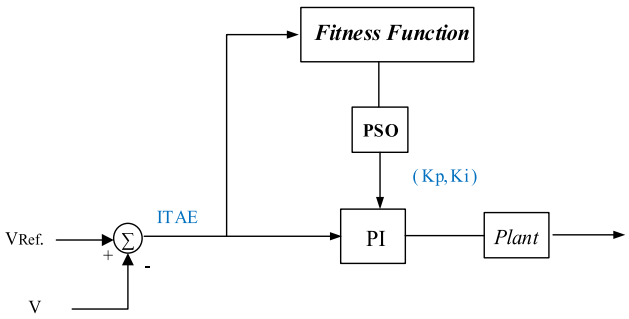

Fig. 5 PSO Parameter Optimization using ITAE

the objective function which is the fitness or cost function to be minimized is the ITAE of the voltage deviation due to a unit step input given as:

$$\text{Fitness}_{\text{ITAE}} = \int_0^{\infty} t.\left|\Delta V_{\text{ref}} - \Delta V(t)\right| \mathrm{d}t \tag{29}$$

The challenge in this study is to minimize at once both performance indicators function in one PSO algorithm. To solve this problem, an ITAE is employed at the output of each source converter. In this way, minimizing the summation implies minimizing each ITAE. Hence our fitness function can be mathematically described as (30):

$$\begin{aligned}
&\text{ITAE 1} = \int_0^{\infty} t.|e(t)|\mathrm{d}t \\
&\text{ITAE 2} = \int_0^{\infty} t.|e(t)|\mathrm{d}t \\
&\text{Fitness}_{\text{ITAE}} = ITAE1 + ITAE2 \\
&\text{Fitness}_{\text{ITAE}} = \int_0^{\infty} t.\left|\Delta V_{\text{ref1}} - \Delta V_1(t)\right|\mathrm{d}t + \int_0^{\infty} t.\left|\Delta V_{\text{ref2}} - \Delta V_2(t)\right|\mathrm{d}t
\end{aligned} \tag{30}$$

The summary of the PI controllers' parameter optimization using PSO is shown in Fig. 6.

Typically, the system's oscillatory response depends on the damping of the system and the mode of the damped natural frequency. Therefore, the optimization function in (31) is defined and minimized using PSO [42] to realize an optimal K_d.

$$\text{Minimize; OF} = \underset{\forall k \in |1,2,\ldots,NST|}{\text{Max}} \left(\text{Real}\lambda_k\}\right) + \sum_{k=1}^{NST} \left(1 - \xi_k\right) \tag{31}$$

where, λ_k is the k^{th} Eigen-value, ξ_k is the damping ratio of the k^{th} Eigen-value, and NST is the number of system states.

The objective function in (31) is realized when the dominant Eigen-value has the largest negative real part and good damping at all modes hence good dynamic response.

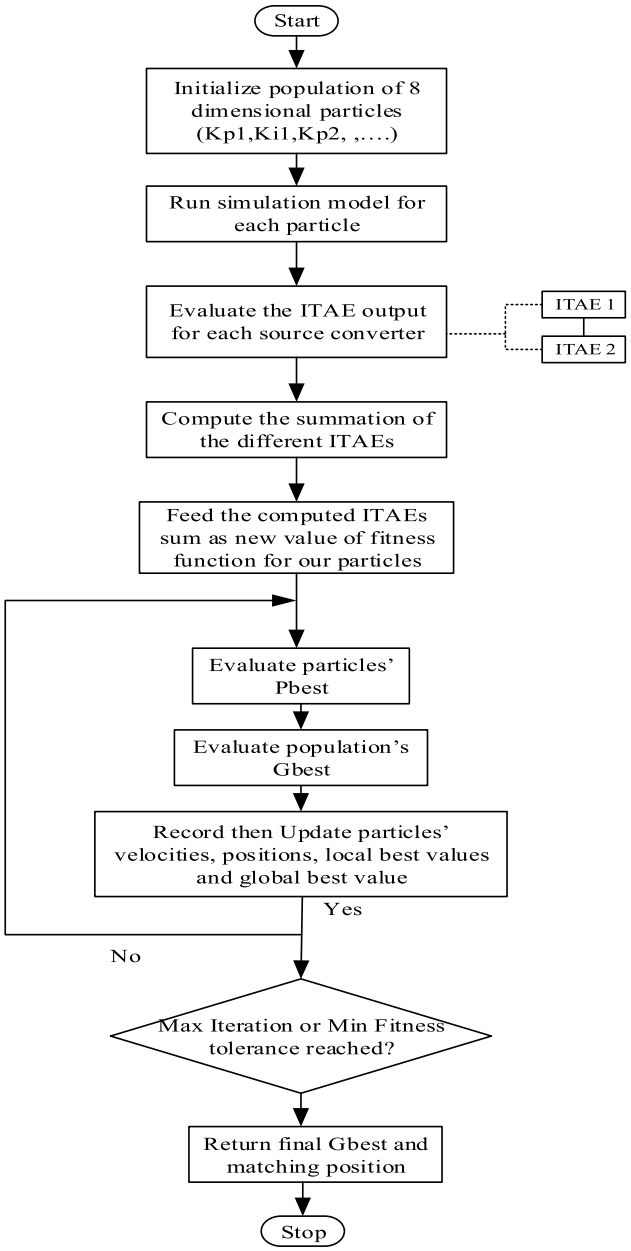

Fig. 6 PSO PI Parameter Optimization

6 Results

6.1 Test System

A scaled-down MVDC distribution network consisting of two identical parallel droop control-based buck converters 1 and 2 supplying a CPL (through buck converter 3) in Fig. 7 is modelled and studied in MATLAB/Simulink. The controllers in Figs. 3, 4 are employed in the source converters during the investigations. Table 1 show the parameters of the MVDC distribution system.

6.2 Influence of CPL Rating on the Large-Signal Stability

Investigations on the effects of CPL power rating on the large-signal stability criterion derived in Sect. 3 are undertaken on the MVDC distribution network. The P_{cpl} rating in the network under the droop control strategy is varied around the maximum allowable P_{cpl} of 943 W obtained in (19). Figure 8 shows the performance of DC voltage and power in the system under varying CPL. Neglecting the starting transients, it can be noted from the output voltage and power of the source converters 1 and 2 as well as

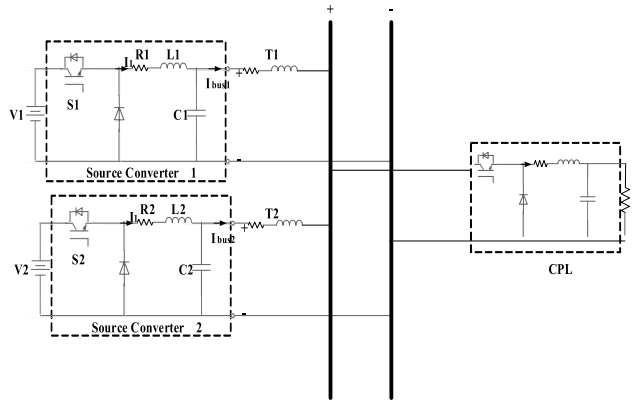

Fig. 7 MVDC Distribution Network for Large-signal Stability Studies

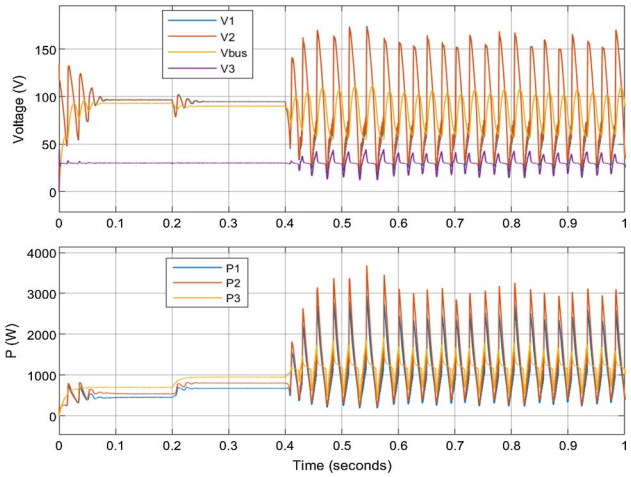

Fig. 8 Influence of increasing CPL rating on Voltage and Power

Table 1 Parameters of the MVDC Network

No	Parameters	Nominal value
1	Buck Input Voltage	200 V
2	Buck Converter Resistance/Inductance	0.2 Ω /0.1e^{-3} H
3	Buck Converter Capacitance	1000e^{-6} μF
4	DC Bus Voltage	100 V
5	Transmission Line along each converter	
	R	0.5 Ω
	L	30e^{-6} H
6	CPL Power (P_{CPL})	700 W
7	Buck Converters1/2 Droop Coefficients:	
	R_{d1}	0.8
	R_{d2}	0.6
8	Outer Controller: PI Parameters	
	K_{vp}	0.1
	K_{vi}	80
9	Inner Controller: PI Parameters:	
	K_{ip}	20
	K_{ii}	100
10	Buck Converter (Load Side): Voltage Controlled	
	K_p	0.1
	K_v	120
11	DC Load Voltage	30 V
12	Converter Switching Frequency	20KHz

the DC bus voltage (V_{bus}) that when the CPL is loaded with the initial 700 W and then a further increase made to 950 W at t = 0.2 s, the system is stable. The CPL loading of 950 W is slightly more than the allowable CPL rating derived from the Brayton-Moser's mixed potential theory for large-signal stability because it provides a sufficient condition for stability. However, when the CPL is increased to 1200 W at t = 0.4 s, the system's bus voltage and power starts to heavily oscillate and does not regain its equilibrium point. In effect as the CPL power rating increases, the system tend towards marginal stability and completely fails when the loading surpasses this point.

6.3 Controller Parameters Variations on the Large-signal Stability

In this case, the effect of varying the droop coefficients of the MVDC distribution system at a constant CPL of 700 W is studied. Figure 9 shows the effect of varying the droop coefficients in the system when the source converters 1 and 2 are considered with increasing droop coefficients (R_d) of 0.1/0.01; 0.5/0.1 and 0.8/0.6 respectively. When the droop coefficient is changed from the lowest values to the middle coefficient set, a voltage drop of about 2.6% is realized. A further increase from the middle set to the highest coefficient set results in a larger voltage drop of about 5.7%. It can be observed that higher droop coefficients have severe impacts on the bus voltage of the system. The study also confirms that a converter with a smaller droop coefficient (converter 1) shares more power.

The influence of variations in the proportional (P) controller coefficients on the voltage and current controllers in the source converters at constant droop coefficient and load displayed in Table 1 are studied. Figure 10 shows the effect of varying the P-value in the DC voltage droop control. The K_{pv} and K_{pi} parameters are varied in increasing order in source converters 1 and 2 as follows; 0.09/15; 0.1/20 and 0.9/30. It can be observed that the start-up oscillations in the MVDC system's voltage and power decreases with increase in the P-parameters.

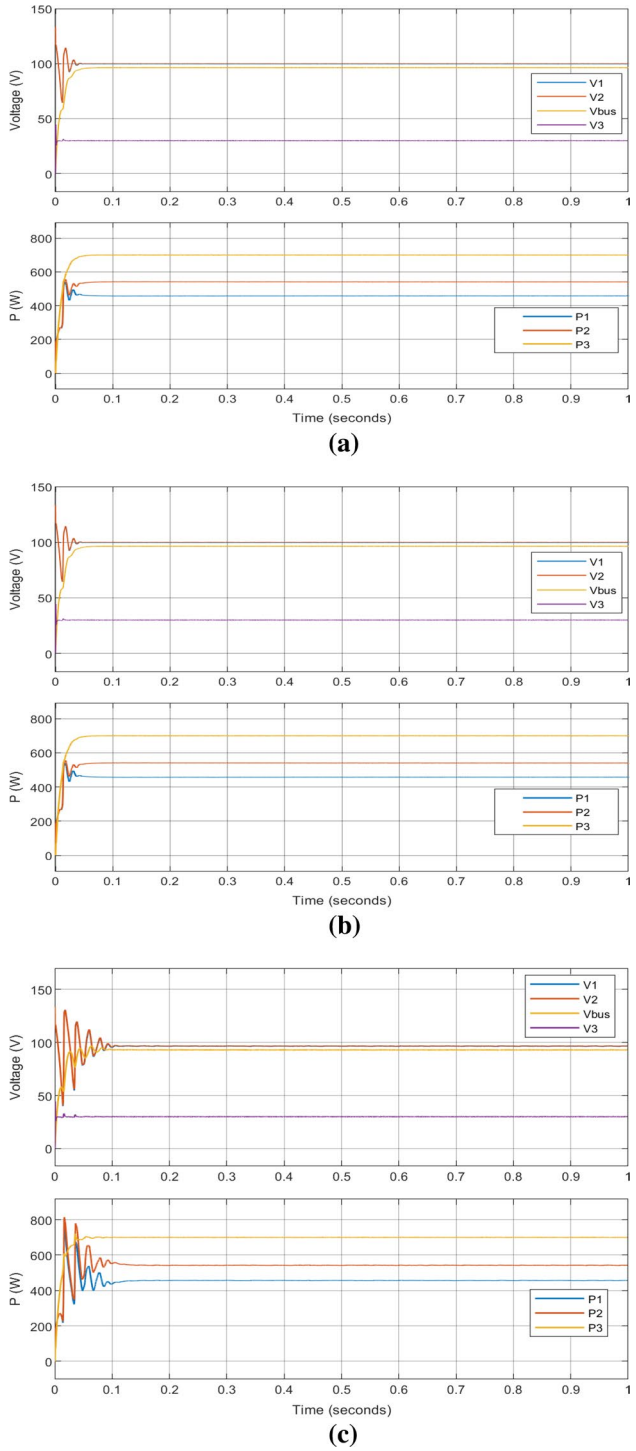

Fig. 9 Effect of increasing Droop Coefficients; (**a**). $R_{d1}/R_{d2}=0.1/0.01$; (**b**). $R_{d1}/R_{d2}=0.5/0.1$ and (**c**). $R_{d1}/R_{d2}=0.8/0.6$

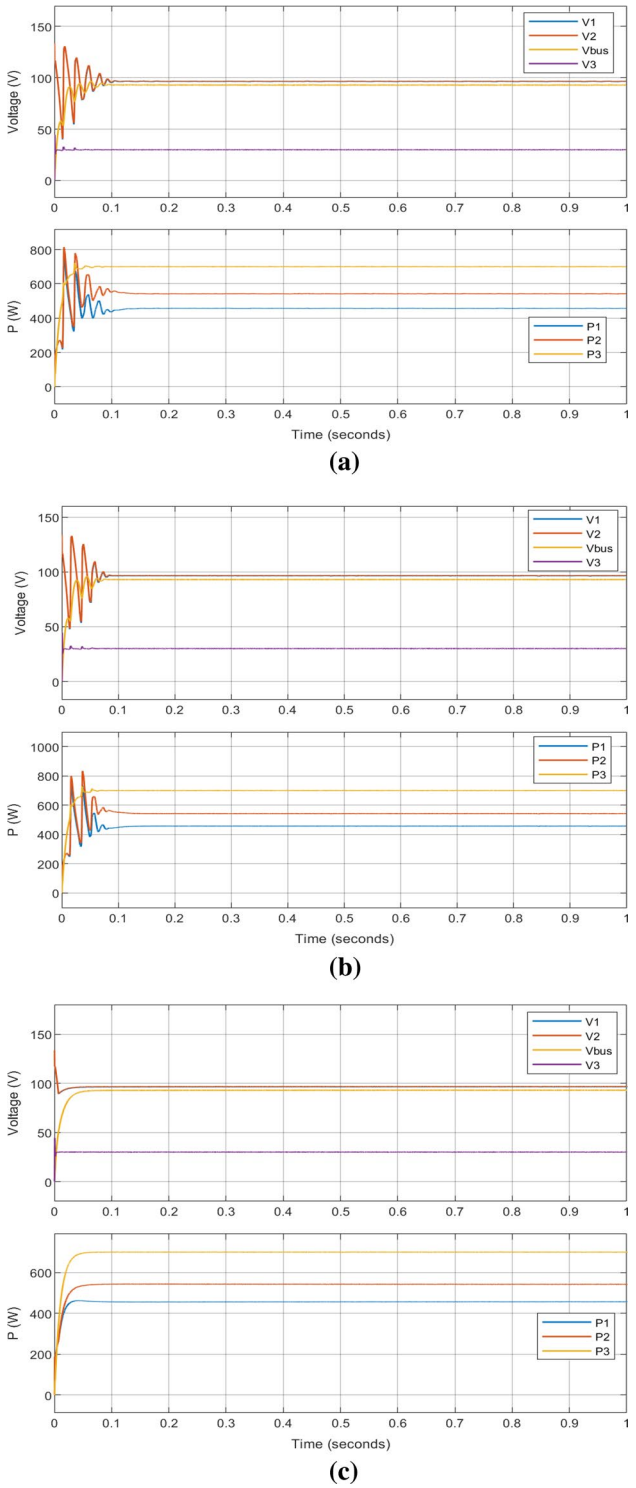

Fig. 10 Effect of increasing Proportional (P) Controller Coefficients; (**a**). $K_{pv}/K_{pi}=0.09/15$; (**b**). $K_{pv}/K_{pi}=0.1/20$ and (**c**). $K_{pv}/K_{pi}=0.9/30$

6.4 Effect of Damping Coefficients on Large-Signal Stability

In this study, the droop-controlled MVDC system with and without virtual inertia are comparatively analyzed with varying loads from 700 W as shown in Fig. 11. The damping coefficients are evaluated as $K_d=0$ (without virtual inertia), $K_d=2$ (un-optimized damping coefficient) and $K_d=5.027$ (optimized coefficient using PSO).

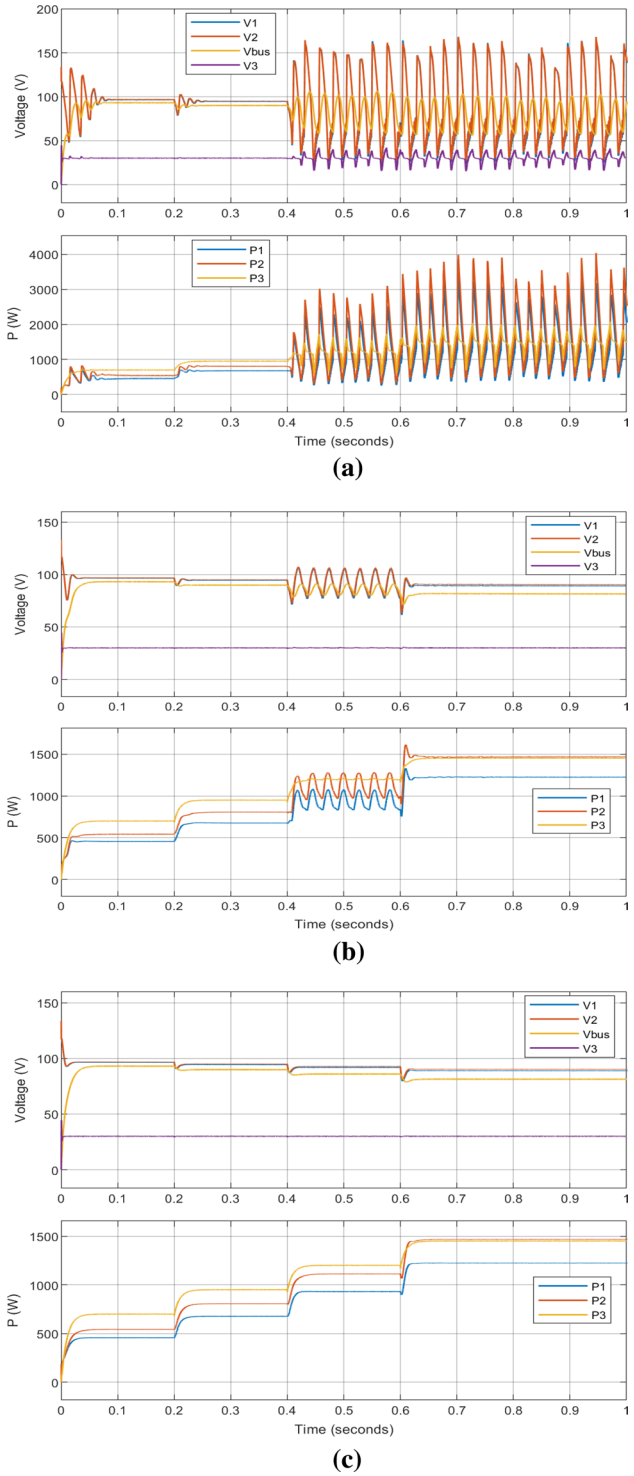

Fig. 11 DC Voltage Droop Control; (**a**). $K_d = 0$ (no inertia) (**b**). $K_d = 2$(un-optimized inertia) (**c**). $K_d = 5.027$ (optimized inertia)

During start-up for about 60 ms, the system without virtual inertia has some significant oscillations in voltage and power at the output of the source converters 1 and 2 as well as the DC bus voltage. In contrast, the system having inertia with a randomly chosen low non-optimized $K_d = 2$ as well as that with an optimized $K_d = 5.027$ has virtually no oscillations during this period.

When the system is loaded to 950 W, 1200 W and 1450 W at t = 0.2 s; t = 0.4 s and t = 0.6 s respectively, intensive voltage and power oscillations are experienced when without virtual inertia. The stability margin of the system is restricted to a CPL rating of about 950 W which is around the 943 W obtained from the large-signal stability criterion in (19). In the system with virtual inertia with un-optimized K_d value, some oscillations are encountered whereas the optimized K_d records none. In this way, when the system is incorporated with virtual inertia having optimized K_d, its large-signal stability margin extends increasing the size of the CPL rating that the system can withstand to about 1450 W which is 1.5 times the CPL rating without virtual inertia.

7 Conclusion

In this study, the large-signal stability criterion of a scaled-down droop-controlled multi-terminal MVDC distribution network with CPL using Brayton-Moser's mixed potential theory was simplified and derived, showing that the CPL power rating, PI control parameters, droop and damping coefficients have profound effects on the system's large-signal stability. By way of MATLAB/Simulink simulations, the large-signal stability of the MVDC distribution system was observed to reduce with increase in CPL power rating and source converter droop coefficients as well as increase with increase in proportionate coefficient values and use of optimized unlike non-optimized damping coefficients. Therefore, the droop-controlled MVDC distribution network with optimized PI control parameters, droop and damping coefficients have enhanced dynamic response and large-signal stability margin proving the accuracy and validity of the simplified large-signal stability criterion.

References

1. Reed GF, Grainger BM, Sparacino AR, Mao Z (2012) Ship to grid: medium-voltage DC concepts in theory and practice. IEEE Power Energ Mag 10(6):70–79
2. Giannakis, A. and D. Peftitsis. MVDC distribution grids and potential applications: future trends and protection challenges. In: 2018 20th european conference on power electronics and applications (EPE'18 ECCE Europe). 2018. Riga, Latvia
3. Hunter, L., C. Booth, S. Finney and A.J. Ferré. MVDC network balancing for increased penetration of low carbon technologies. In: 2018 IEEE PES innovative smart grid technologies conference Europe (ISGT-Europe). 2018. Sarajevo, Bosnia-Herzegovina

4. Gómez-Expósito A, Mauricio JM, Maza-Ortega JM (2014) VSC-Based MVDC railway electrification system. IEEE Trans Power Delivery 29(1):422–431
5. Stieneker M, Doncker RWD. Medium-voltage DC distribution grids in urban areas. In: 2016 IEEE 7th international symposium on power electronics for distributed generation systems (PEDG). 2016. Vancouver, BC, Canada
6. Reed GF, Grainger BM, Korytowski MJ, Taylor EJ Modeling, analysis, and validation of a preliminary design for a 20 kV medium voltage DC substation. In: IEEE 2011 EnergyTech. 2011. Cleveland, OH, USA
7. Korompili A, Sadu A, Ponci F, Monti A flexible electric networks of the future: project on control and automation in MVDC grids. In: International ETG Congress 2015; Die Energiewende—Blueprints for the new energy age. 2015. Bonn, Germany.
8. Huang Z, Ma J, Zeng J, Gao Y, Yuan Z, Hu Z, Zhao Y, Liu G. Research status and prospect of control and protection technology for DC distribution network. In: 2014 China international conference on electricity distribution (CICED). 2014. Shenzhen, China.
9. IEEE, IEEE recommended practice for electronic power subsystems: parameters, interfaces, elements, and performance. IEEE Std 1573–2003, 2004: pp 0_1–115.
10. Emadi A, Khaligh A, Rivetta CH, Williamson GA (2006) Constant power loads and negative impedance instability in automotive systems: definition, modeling, stability, and control of power electronic converters and motor drives. IEEE Trans Veh Technol 55(4):1112–1125
11. Smithson SC, Williamson SS Constant power loads in more electric vehicles—an overview. In: IECON 2012—38th annual conference on IEEE industrial electronics society. 2012. Montreal, QC, Canada
12. Riccobono A, Cupelli M, Monti A, Santi E, Roinila T, Abdollahi H, Arrua S, Dougal RA (2017) Stability of shipboard DC power distribution: online impedance-based systems methods. IEEE Electrification Magazine 5(3):55–67
13. Dragičević T, Lu X, Vasquez JC, Guerrero JM (2016) DC microgrids—Part I: a review of control strategies and stabilization techniques. IEEE Trans Power Electron 31(7):4876–4891
14. Simiyu P, Xin A, Bitew GT, Shahzad M, Kunyu W, Kamunyu PM (2019) Small-signal stability analysis for the multi-terminal VSC MVDC distribution network; a review. J Eng 2019(16):1068–1075
15. Amin M, Molinas M (2017) Small-signal stability assessment of power electronics based power systems: a discussion of impedance- and eigenvalue-based methods. IEEE Trans Ind Appl 53(5):5014–5030
16. Kim H, Kang S, Seo G, Jang P, Cho B (2016) Large-signal stability analysis of dc power system with shunt active damper. IEEE Trans Industr Electron 63(10):6270–6280
17. Du W, Zhang J, Zhang Y, Qian Z (2013) Stability criterion for cascaded system with constant power load. IEEE Trans Power Electron 28(4):1843–1851
18. Marx D, Magne P, Nahid-Mobarakeh B, Pierfederici S, Davat B (2012) Large signal stability analysis tools in DC power systems with constant power loads and variable power loads—a review. IEEE Trans Power Electron 27(4):1773–1787
19. Kabalan M, Singh P, Niebur D (2017) Large signal lyapunov-based stability studies in microgrids: a review. IEEE Trans Smart Grid 8(5):2287–2295
20. Loop BP, Sudhoff SD, Żak SH, Zivi EL (2010) Estimating regions of asymptotic stability of power electronics systems using genetic algorithms. IEEE Trans Control Syst Technol 18(5):1011–1022
21. Bacha A, Jerbi H, Braiek NB An approach of asymptotic stability domain estimation of discrete polynomial systems. In: The proceedings of the multiconference on "computational engineering in systems applications". 2006. Beijing, China
22. Weaver WW, Robinett RD, Wilson DG, Matthews RC (2017) Metastability of pulse power loads using the hamiltonian surface shaping method. IEEE Trans Energy Convers 32(2):820–828
23. Weiss L, Mathis W, Trajkovic L (1998) A generalization of Brayton-Moser's mixed potential function. IEEE Trans Circuits Syst I: Fundamental Theory Appl 45(4):423–427
24. Jeltsema D, Scherpen JMA (2005) On Brayton and Moser's missing stability theorem. IEEE Trans Circuits Syst II Express Briefs 52(9):550–552
25. Belkhayat M, Cooley R, Witulski A Large signal stability criteria for distributed systems with constant power loads. In: Proceedings of PESC '95—power electronics specialist conference. 1995. Atlanta, GA, USA.
26. Che Y, Xu J, Shi K, Liu H, Chen W, Yu D (2017) Stability analysis of aircraft power systems based on a unified large signal model. Energies. 10(11).
27. Griffo A, Wang J (2012) Large signal stability analysis of 'more electric' aircraft power systems with constant power loads. IEEE Trans Aerosp Electron Syst 48(1):477–489
28. Griffo A, Wang J, Howe D Large signal stability analysis of DC power systems with constant power loads. In: 2008 IEEE vehicle power and propulsion conference. 2008. Harbin, China
29. Liu X, Zhou Y, Zhang W, Ma S (2011) Stability criteria for constant power loads with multistage LC Filters. IEEE Trans Veh Technol 60(5):2042–2049
30. Huang M, Ji H, Sun J, Wei L, Zha X (2017) Bifurcation-based stability analysis of photovoltaic-battery hybrid power system. IEEE J Emerging Selected Topics Power Electron 5(3):1055–1067
31. Huang M, Peng Y, Tse CK, Liu Y, Sun J, Zha X (2017) Bifurcation and large-signal stability analysis of three-phase voltage source converter under grid voltage dips. IEEE Trans Power Electron 32(11):8868–8879
32. Tamrakar U, Shrestha D, Maharjan M, Bhattarai PB, Hansen MT, Tonkoski R (2017) Virtual inertia: current trends and future directions. Applied Sciences. 7(7).
33. Hosseinipour A, Hojabri H (2018) Virtual inertia control of PV systems for dynamic performance and damping enhancement of DC microgrids with constant power loads. IET Renew Power Gener 12(4):430–438
34. Soni N, Doolla S, Chandorkar MC (2013) Improvement of transient response in microgrids using virtual inertia. IEEE Trans Power Delivery 28(3):1830–1838
35. Zhu X, Cai J, Yan Q, Chen J, Wang X Virtual inertia control of wind-battery-based islanded DC micro-grid. In: International Conference on Renewable Power Generation (RPG 2015). 2015. Beijing, China.
36. Simiyu P, Xin A, Wang K, Adwek G, Salman S Multiterminal Medium Voltage DC Distribution Network Hierarchical Control. Electronics, 2020. 9(3).
37. Jiang J, Liu F, Pan S, Zha X, Liu W, Chen C, Hao L (2019) A conservatism-free large signal stability analysis method for DC microgrid based on mixed potential theory. IEEE Trans Power Electron 34(11):11342–11351
38. Severino B, Strunz K (2019) Enhancing transient stability of DC microgrid by enlarging the region of attraction through nonlinear polynomial droop control. IEEE Trans Circuits Syst I Regul Pap 66(11):4388–4401
39. Cleghorn CW, Engelbrecht AP Particle swarm convergence: An empirical investigation. In: 2014 IEEE Congress on Evolutionary Computation (CEC). 2014. Beijing, China
40. Shi Y, Eberhart R A modified particle swarm optimizer. In: 1998 IEEE international conference on evolutionary computation proceedings. IEEE world congress on computational intelligence (Cat. No.98TH8360). 1998. Anchorage, AK, USA.
41. Shi Y, Eberhart RC. Empirical study of particle swarm optimization. In: Proceedings of the 1999 congress on evolutionary

computation-CEC99 (Cat. No. 99TH8406). 1999. Washington DC, USA
42. Maulik A, Das D (2019) Stability constrained economic operation of islanded droop-controlled DC microgrids. IEEE Transactions on Sustainable Energy 10(2):569–578

Patrobers Simiyu received a Bachelor of Education (Technology Education) at Moi University, Kenya in 2004. He received an MSc in Energy Technology at Jomo Kenyatta University of Agriculture & Technology, Kenya in 2016. He joined North China Electric Power University (NCEPU), Beijing in 2015 to 2020 for a Ph.D. in Electric Power System and its Automation. He is a Lecturer at the Department of Electrical and Electronic Engineering, Kenya-Coast National Polytechnic since 2008. His research interests are in Modeling and Control of Flexible Energy Networks and Power System Stability.

Ai Xin received the B.S. degree from the Nanjing Institute of Technology, Southeast University, Nanjing, China, the M.S. degree from China Electric Power Research Institute, Beijing, China, and the Ph.D. degree from North China Electric Power University (NCEPU), Beijing, in 1985, 1988, and 1999, respectively, all in Electrical Engineering. He was a Senior Research Scholar with Brunel University, London, U.K., in 2003. He is the Director of the Research Center for Power Systems, NCEPU, where he is involved in research and teaching in Power System and its Automation. He is currently a Professor and a Doctoral Tutor with the School of Electrical and Electronic Engineering, NCEPU. His current research interests include Power System Analysis and Control, New Energy, and Microgrid Power Systems.

Niasse Mouhammed received his Master of Electro-mechanical Engineering degree (Diplôme d'ingénieur de conception) from Ecole Polytechnique de Thiès in Senegal in 2016. He is currently undertaking his Ph.D. in Electrical Engineering at North China Electric Power University (NCEPU) Beijing from 2017. His research focus is on power system frequency stability and integration of hydropower in large-scale power systems.

Wang Kunyu received the B.S. and M.S. degrees in Electrical Engineering from North China Electric Power University (NCEPU), Beijing in 2012 and 2016 respectively. He is currently pursuing a Ph.D. in Electrical Engineering at NCEPU.

Joseph Gurti received the B.S. from the University of Dar es salaam, Tanzania in 2018. He joined the North China Electric Power University (NCEPU), Beijing in 2019 where he is pursuing his Master's degree.